Journal of Imaging Science and Technology® 66(4): 040414-1–040414-11, 2022.

Ultrasonic Image Optimization based on Double Constraint Algorithm

Shuai Zhang
School of Information Science and Engineering, Yanshan University, Qinhuangdao 066004, Hebei, China
Hebei Normal University of Science & Technology, Qinhuangdao 066004, Hebei, China

Caiyan Pei and Dejie Sun
Hebei Normal University of Science & Technology, Qinhuangdao 066004, Hebei, China

Jian Wang
Xinzhou Teachers University, Xinzhou 034000, Shanxi, China

Wenyuan Liu
School of Information Science and Engineering, Yanshan University, Qinhuangdao 066004, Hebei, China
E-mail: wyliu@ysu.edu.cn

Abstract. *The study of ultrasonic image deblurring is of high research value and practical significance, which can provide significantly useful medical pathological information for doctors and patients. Ultrasonic images are prone to speckle noise or blur. Real-time deblurring of ultrasonic images is a common problem in medical circles in China and globally. In this paper, based on the causes of ultrasound image degradation and its degradation model, the problem of ultrasound image deblurring is studied in depth. A new regularization constraint model is given, and the algorithm of ultrasound image deblurring with double constraints is effective. Through the experiment, the image quality evaluation index is used to evaluate the experimental results. The improved algorithm proposed in this paper improves the peak signal-to-noise ratio by 7%, the structural similarity value by 6%, the visual information fidelity by 14%, the feature similarity value by 4%, the resolution gain by 4%, and the new blind image quality evaluation value by 22%. The key information of the image can be kept faithfully. Compared with the traditional methods, the proposed method enhances the identification of the focus area in ultrasound images, provides a fast, efficient and complete deblurring method for medical image analysis, and faithfully retains and restores the required information in ultrasound images.*

[DOI: 10.2352/J.ImagingSci.Technol.2022.66.4.040414]

1. INTRODUCTION

Digital image deblurring has developed rapidly, which effectively solves the problem of low imaging quality of medical ultrasound images. It explores the causes of image degradation from the root and establishes its mathematical model. Digital image deblurring is mainly divided into two categories: non-blind deblurring and blind deblurring. Non-blind deblurring means that the blurred image and fuzzy kernel are known and the clear image is recovered by deconvolution; blind deblurring means that only the blurred image is known while the clear image and fuzzy kernel are unknown. The clear image and fuzzy kernel are estimated by using the observation data of the blurred image and limited prior knowledge [1]. In practical application, the degradation process of the medical ultrasound imaging systems is difficult to describe accurately. Hence, the blind deblurring algorithm is typically used.

Image blind deblurring algorithm is a technology that only uses the blurred image to restore the image and estimate the fuzzy kernel when the cause of image degradation is unknown. It has important theoretical and practical significance. For the blind deblurring algorithms of medical images, most of the current algorithms have some limitations, such as high computational complexity and lack of real-time performance. Therefore, the method of obtaining blind deblurring algorithm of medical images efficiently is the focus of this research. The research on how to use digital image technology to improve the imaging quality of the ultrasonic images has far-reaching scientific significance and practical value [2].

Because the overall color of the ultrasound image is dark, and the difference in the pixel value weights of some regions in RGB channels is large, it is easy to cause inaccurate estimation of the blur kernel and the deblurred image by directly using the prior information obtained from the converted grayscale image.

Many scholars use traditional image deblurring algorithms, such as linear deblurring algorithms: Wiener filter, total variation method, constrained least squares filter; nonlinear deblurring algorithm: maximum a posteriori deblurring algorithm and maximum entropy deblurring algorithm based on Bayesian theory have also achieved certain results in ultrasonic image deblurring [3]. Sun et al. [4] used the impulse filter to select the edge to obtain

Received Nov. 26, 2021; accepted for publication May 14, 2022; published online Aug. 1, 2022. Associate Editor: Bo Wang.
1062-3701/2022/66(4)/040414/11/$25.00

the module prior information, and then iteratively restored the blurred image and fuzzy kernel. In 2016, Zhao et al. [5] studied a post-processing method to reverse the direct linear model of ultrasonic imaging, which can calculate the analytical solution of the 2L norm regular stochastic resonance problem. In 2016, Pan et al. [6] used the sparsity prior of bright or dark channels to construct regular terms. In 2017, Gong et al. [7] did not try to identify the outliers of the model, but proposed to identify the outliers sequentially and gradually incorporate them into the estimation process. In this method, kernel estimation is carried out by gradually detecting and including reliable pixel inner sets in the blurred image. In 2018, Liao et al. [8] proposed a fuzzy kernel estimation model based on combined constraints, which uses L^0 regularization terms to constrain image gradient and image dark channel so as to protect the strong edge of the image and suppress the noise in the image. It uses the 2L regularization term as the mixed beam of the Fuzzy kernel and its gradient to maintain the sparsity and continuity of the fuzzy kernel respectively. In 2019, Chen et al. [9] proposed a blind deblurring method based on a prior local maximum gradient (LMG), which calculates the local maximum gradient and an effective optimization scheme by introducing a linear operator. In 2020, Zhou et al. [10] proposed a joint prior model for the case that the pixel values of the dark channel and bright channel in some images are not concentrated on 0 and 1 respectively. The model combines the prior extreme channel and L^0 normalized intensity and gradient to remove the blur of blind images. In 2021, Yang et al. [11] proposed an effective blind image deblurring method based on a reweighted L^1 norm, which uses a reweighted L^1 norm to eliminate its dependence on the weighting range of bright elements.

A double constrained ultrasonic image deblurring algorithm is proposed in this paper. As is known, the overall tone of the ultrasonic image is dark and the pixel weight difference of some regions in the RGB channel is large. Besides, the extraction of the prior information of the image depends on the edge information, and the prior information obtained by directly using the converted gray image is easy to cause problem of inaccurate estimation of the fuzzy kernel. Based on the difference between quadratic sparse dark channel and quadratic sparse bright channel, an improved edge selection method is proposed to improve the accuracy of edge extraction. At the same time, combined with L^1 norm and L^2 norm, a double constrained ultrasonic image deblurring algorithm is proposed. The adaptive weighting space is combined when the ultrasonic image is finally restored so that it can retain its sharp edges more effectively.

The main innovations of this paper are as follows:

The quadratic sparse bright channel is proposed in this paper, and a prior of the quadratic sparse extreme channel is obtained by combining the two.

The difference between quadratic sparse dark channel and quadratic sparse bright channel is used to improve the edge selection method.

A new ultrasonic image deblurring algorithm with double constraints is proposed.

Main contents of each section:

Section 1 introduces the research progress of ultrasonic image denoising.

Section 2 introduces the theoretical basis of this study.

Section 3 discusses the gradient space calculation of ultrasonic images.

Section 4 introduces a double-constrained ultrasonic image deblurring model.

Section 5 discusses the experiment and analysis.

Section 6 summarizes this paper and looks forward to future development.

2. RELATED TECHNOLOGY

Due to the random disturbance of electronic devices in the acquisition equipment of ultrasonic imaging and the influence of the surrounding environment, many irregular speckle noises often appear in the ultrasonic images of human tissues and organs, which reduces the contrast between the target area and the background area in the image, making it sometimes difficult for people to distinguish the focus information, background information and noise information. It greatly affects image quality and lesion recognition. This paper mainly focuses on the causes of ultrasonic image blur and performance evaluation metrics.

2.1 *Causes of Ultrasonic Image Blur*

Although the actual ultrasonic imaging system is very complex, the ultrasonic image is considered to be the blur of the ideal image in the actual processing in general. Therefore, it is regarded as a conventional image degradation system. Its degradation model is consistent with the conventional image degradation model. The prior distribution of the ultrasonic image is consistent with the gray gradient distribution of the natural image, both of which obey the heavy tail distribution. Because it meets the super Laplace distribution, the deconvolution model for digital image deblurring can basically be used for ultrasonic image deblurring [12]. However, since medical ultrasound images have some different features from general digital images, it is necessary to analyze the characteristics of medical ultrasound images and add this prior information to the deconvolution algorithm to obtain an algorithm image suitable for ultrasonic image deblurring [13]. The fuzzy degradation process of the ultrasonic images can be expressed as:

$$B = I \otimes k + n. \tag{1}$$

B represents the blurred image; I represents the clear image; k is the fuzzy kernel; n is the noise and $\otimes$ is the convolution operator. Because B can be generated by different I and k, it is an ill posed problem and the solution is more complex.

As for image I, convolution is defined as:

$$b(x) = \sum_{s=21\times x} I\left(x + \left[\frac{s}{2}\right] - z\right) k(s). \tag{2}$$

(x) represents the image module centered on pixel x whose size is the same as that of fuzzy kernel. Z represents rounding operator. According to the properties of fuzzy kernel, we can obtain:

$$k(s) \geq 0; \quad \sum_{k=0} k(s) = 1.$$

2.2 *Performance Evaluation Metric*

With the rapid development of digital image technology, in the process of image acquisition, transmission and recovery, the image may have distortion problems such as blur or noise. At this time, it is unreasonable to only rely on people's subjective feelings to evaluate the image [14]. In recent years, many scholars have done a lot of research on image quality evaluation. There are two kinds of image quality evaluation methods: subjective evaluation and objective evaluation. Subjective evaluation means that the observer visually observes the image with his eyes and evaluates the image quality according to his subjective opinions. Therefore, the results of the subjective evaluation are very different and the application prospect is narrow. Objective evaluation refers to the index of image quality evaluation obtained by a computer. The presence or absence of a reference image, it can be divided into three categories: Full Reference (FR), Reduced Reference (RR) and No Reference (NR). The image quality evaluation methods of FR and RR require distortion-free images, but it is difficult to obtain distortion-free images with "perfect" quality in real life [15]. The objective image quality evaluation is mainly evaluated by obtaining some feature information of the image, such as texture features, edge features, shape features and so on. Therefore, the application prospect of objective image quality evaluation is good. Ultrasonic image quality evaluation belongs to objective quality evaluation [16]. Full reference image quality evaluation is mainly to calculate the difference between the reference image and deblurring image. Common indicators include mean square error (MSE), Signal to-Noise Ratio (SNR) [17], Peak Signal-to-Noise Ratio (PSNR), Structural Similarity Index (SSIM) and Feature Similarity (FSIM) And Visual Information Fidelity (VIF) [18]. Part of the reference image quality evaluation mainly takes some features of the undistorted image as the reference so as to compare and analyze the deblurring images. Common indicators include methods based on original image features and methods based on Wavelet domain statistical model [19]. No reference image quality evaluation is a quality evaluation method completely separated from the reference image. The common indicators include meaning, standard deviation, entropy and so on. With the research on blind image deblurring algorithm, more and more scholars propose to update the non- reference image quality evaluation indexes, such as Resolution Gain (RG) and Blind Image Quality Indexes (BIQI) [20].

2.2.1 *Peak Signal-to-Noise Ratio*

The mean square error (MSE) of the image refers to the square difference between the original (input) image pixel and the deblurring (output) image pixel, and its calculation formula is defined as follows:

$$MSE = \frac{1}{m \times n} \sum_{i=0}^{m-1} \sum_{j=0}^{n-1} |I(i,j) - I'(i,j)|^2. \tag{3}$$

I and I' are the original image and the deblurring image respectively. $m \times n$ represents the size of the image. The smaller the MSE value, the more similar the original image and the deblurring image are.

Peak signal-to-noise ratio (PSNR) is a benchmark method to evaluate the effectiveness of other image quality indicators. It is used to calculate the ratio of the maximum possible square Max2 of the original image or deblurring image to the corresponding MSE in decibels. Its calculation formula is defined as follows:

$$PSNR = 10 \log_{10} \left(\frac{\max^3}{1\sqrt{MSE}} \right). \tag{4}$$

For uint8 ultrasonic image data, the maximum possible value Max is 255.

2.2.2 *Structural Similarity*

Structure similarity (SSIM) measures the similarity between the original image I and the deblurring image I' by considering three different components: structure, brightness and contrast. Its calculation formula is defined as follows:

$$i(I, I') = \frac{2k_1 t_1 + c_1}{k_1^2 + k_1^2 + c_1} \tag{5}$$

$$c(I, t') = \frac{20_T + c_2}{\sigma_I^3 + \sigma_1^3 + C_2} \tag{6}$$

$$s(I, t') = \frac{\partial_J + c_3}{\partial_f t^{O_f + c_3}}. \tag{7}$$

σ_I and ∂_I represents the mean and standard deviation of I. $\sigma_{I'}$ and $\partial_{I'}$ represents the mean and standard deviation of I'. $\sigma_{II'}$ represents the covariance of I and I'. $C1$, $C2$ and $C3$ are constants, which are used to avoid instability when the denominator is very close to zero.

2.2.3 *Feature Similarity*

Feature similarity (FSIM) is coupled by PC term and GM term. In this paper, PC and GM are calculated by reference [21]. Assuming that the similarity between images I_1 and I_2 is calculated, firstly, the feature similarity measure between image $I_1(x)$ and $I_2(x)$ is divided into two components. Each component is used for PC or GM. And then, $S_{pc}(x)$ and $S_G(x)$ are combined to obtain the similarity $S_L(x)$ of $I_1(x)$ and $I_2(x)$.

$$S_{pc}(x) = \frac{2PC_1(x)PC_1(x) + T_1}{PC_1^2 + P_2^2 + T_1} \tag{8}$$

$$S_G(X) = \frac{2G_1(x)G_2(x) + T_3}{G_1(x)^2 + G_2(x)^3 + T_2} \tag{9}$$

$$S_L(x) = [S_{PC}(x)]^{\alpha}[S_G(x)]^{\theta}. \tag{10}$$

PC_1 and PC_2 represent PC maps extracted from I_1 and I_2. G1 and G2 represent GM maps extracted from them. Therefore, the calculation formula of FSIM is defined as follows:

$$\mathrm{FSIM} = \frac{\sum_{x\in a} S_L(x)PC_m(x)}{\sum_{x=a} PC_m(x)}. \tag{11}$$

α represents the entire image space domain.

2.2.4 *Information Fidelity Criterion*

The information fidelity criterion (VIF) quantifies the Shannon information shared between the reference image and the distorted image relative to the information contained in the reference image itself. The score of the reference image information extracted from the test image is also contained [22]. It is assumed that each subband is completely independent of other subbands in terms of RF and distortion model parameters. Therefore, visual information fidelity (VIF) is defined as follows:

$$\mathrm{VIF} = \frac{\sum_{j\in\text{subbands}} I(C^{N,j}; F^{N,j})}{\sum_{j\in\text{subbands}} I(C^{N,J}; E^{N,J})}. \tag{12}$$

$C^{N,j}$ represents the n elements of RF and C_j, which describe the coefficients of subband j.

2.2.5 *Resolution Gain*

The resolution gain (RG) evaluates the effect of the deblurring image by comparing the ratio of the original image I to the number of pixels of the deblurring image I' whose normalized autocorrelation coefficient is greater than the given threshold t. Its calculation formula is defined as follows:

$$\mathrm{RG} = \frac{\mathrm{sum}(\mathrm{corrcoef}(I') > t)}{\mathrm{sum}(\mathrm{corrcoef}(I) > t)} \tag{13}$$

$\mathrm{corrcoef}(I)$ and $\mathrm{corrcoef}(I')$ represent the autocorrelation functions of I and I' respectively. If $\mathrm{RG} > 1$, the quality of deblurring image is improved. The higher the RG value, the better the image quality. Generally, the threshold t is set to 0.75. But when the image distortion is weak, the threshold t needs to be increased [23].

2.3 *Blind Image Quality Index*

Given a distorted image, the algorithm first estimates that there is a set of distortion in the image. In demonstration, this group is composed of JPEG, JPEG2000 (JP2k), white noise (WN), Gaussian blur (blur) and fast fading (FF) [24]. And expressed as $p_i = \{i = 1, \ldots, 5\}$. The first stage is essentially a classification stage. The second stage evaluates the quality of the image along these distortions. Let $q_i = \{i = 1, \ldots, 5\}$ represents the quality score of each of the five quality evaluation algorithms [25]. The quality of the image is expressed as probability weighted summation:

$$\mathrm{BIQI} = \sum_{5}^{i=1} p_i \cdot q_i. \tag{14}$$

In this paper, six Image Quality Assessment (IQA) indexes are used to evaluate the experimental results. They are PSNR, SSIM, VIF, FSIM, RG and BIQI respectively.

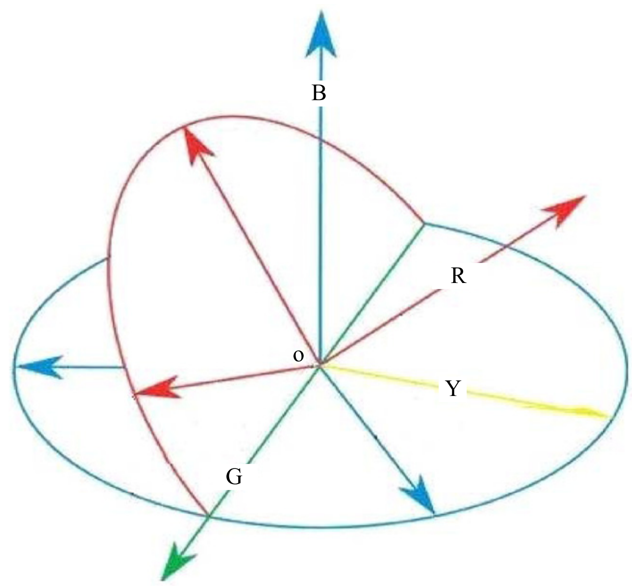

Figure 1. RGB color cube.

2.4 *Adaptive Weighted Space*

The Euclidean distance of a sample pair in a high-dimensional space is normalized and then grouped and analyzed according to different distribution conditions of the distance. Adaptive weighting processing is carried out when similar probability between sample points in the high-dimensional space is calculated according to three conditions of short distance, moderate distance and long distance respectively. The weighted relative distance is used for replacing the Euclidean absolute distance to measure the similarity degree of each group of different samples in a high-dimensional space more truly.

Calculate the joint probability of the high-dimensional space sample pair based on the weighted distance. The joint probability remains unchanged for low-dimensional samples within a two-dimensional space. The objective function is constructed by the two joint probabilities, and then the low-dimensional expression corresponding to the input data is differentiated by the objective function. The low-dimensional expression is used as an optimizable variable for optimization so that the optimal simulation point of the high-dimensional input value in the low-dimensional space is obtained, and the dimensionality reduction and clustering visualization results of the high-dimensional brain network sample are realized.

3. GRADIENT SPACE CALCULATION OF ULTRASONIC IMAGE

RGB color space is transformed into RGB orthogonal color space with color constancy. The gradient of color ultrasonic image is introduced into RGB orthogonal color space. And an edge selection method is used by the difference between quadratic sparse dark channel and quadratic sparse bright channel.

3.1 *RGB Orthogonal Ultrasonic Space*

Figure 1 shows the RGB ultrasonic spatial model, in which each point can represent different colors.

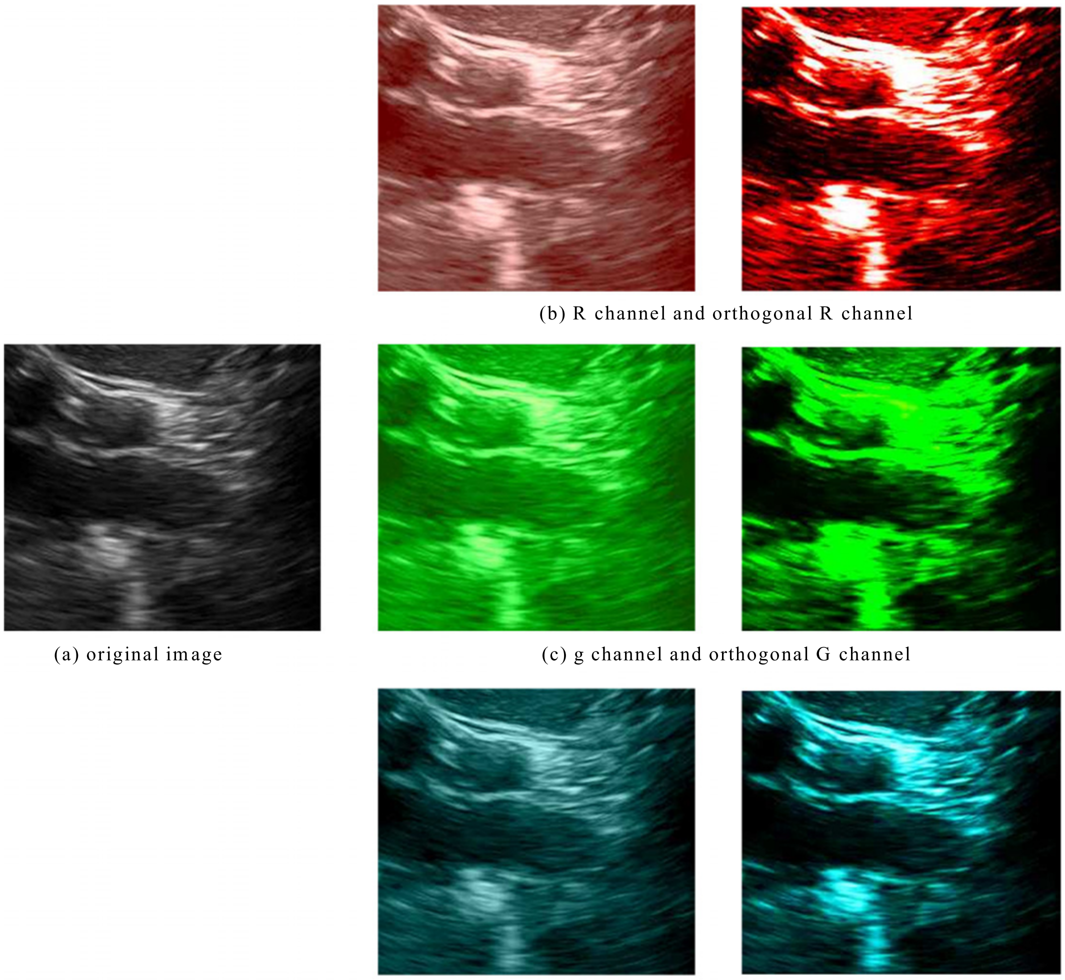

(b) R channel and orthogonal R channel

(a) original image

(c) g channel and orthogonal G channel

(d) B channel and orthogonal B channel

Figure 2. Comparison between RGB color space and RGB orthogonal color space.

The gray image is represented by the points on the black-and-white line of the RGB color cube. The RGB orthogonal ultrasonic space is represented by the plane perpendicular to the black-and-white line.

Figure 2 shows the original ultrasonic image and its images on R, G and B channels and orthogonal R, G and B channels respectively.

The color difference of images in RGB orthogonal space is more obvious in different regions. Therefore, RGB orthogonal ultrasonic space is selected for gradient extraction of image edges [17].

3.2 *Ultrasonic Image Gradient Calculation*

For an image I, the method of extracting image gradient in this paper is as follows:

(1) The ultrasonic image I is transformed into RGB orthogonal color space by formula (15) in which I^R, I^G and I^B are the R, G and B channels corresponding to I respectively.

$$[r, g, b] = \left[\frac{I^R}{I^R + I^G + I^B}, \frac{I^G}{I^R + I^G + I^B}, \frac{I^B}{I^R + I^G + I^B}\right]. \tag{15}$$

(2) The horizontal and vertical gradients of the three channels of RGB orthogonal color space are obtained respectively. Formula (16) gives the horizontal and vertical gradient operators used in this method. Formulas (17)–(19) are the calculation methods of the horizontal and vertical gradients of orthogonal R, G and B channels respectively [26].

$$f_x = \begin{bmatrix} 1/12 & 1/6 & 1/6 & 1/6 \\ -1/12 & -1/6 & -1/6 & -1/12 \end{bmatrix} f_x = f_x^n \tag{16}$$

$$r_x = r(\theta) f_x, r_y = r(\theta) f_y \tag{17}$$

$$g_x = g \otimes f_x; g_y = g \otimes f_y \tag{18}$$

$$b_x = b \otimes f_x; b_y = b \otimes f_y. \tag{19}$$

In the color cube shown in Fig. 1, if we assume that its unit vector is $\bar{i}, \bar{j}, \bar{k}$, the vector u, v in the RGB orthogonal ultrasonic space can be defined as:

$$u = r_x i + g_x j + b_x k \tag{20}$$

$$v = r_y i + g_y j + b_y k. \tag{21}$$

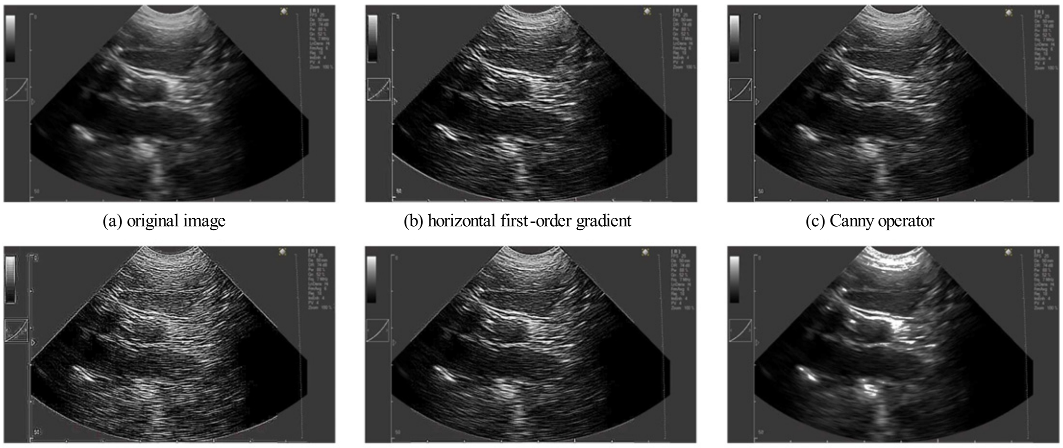

(a) original image (b) horizontal first-order gradient (c) Canny operator

(d) Sobel operator (e) Laplas gradient operator (f) Edge selection

Figure 3. Image edges extracted in 5 ways.

(1) Use the gradient values of orthogonal R, G and B to solve the dot product of the vector **u**, **v**:

$$A_1 = |r_x|^2 + |g_x|^2 + |b_x|^2 + |v_x|^2 \tag{22}$$

$$A_2 = |r_v|^2 + |g_v|^2 + |b_v|^2 \tag{23}$$

$$A_3 = r_x r_y + g_x g_y + b_x b_y. \tag{24}$$

(2) The direction θ of the maximum rate of change can be solved by formula (25):

$$\theta = \frac{1}{2} \arctan \frac{2A_3}{A_1 - A_3}. \tag{25}$$

(1) The ultrasonic image gradient is obtained by substituting θ into formula (26):

$$\theta^c = \sqrt{A_1 \cos^2 \theta + A_2 \cos^2 \theta + A_3 \theta + A_3 \sin 2\theta}. \tag{26}$$

3.3 *Edge Selection*

The greater the brightness change of the image, the clearer the edge. Therefore, using the local information of secondary sparse dark channel and secondary sparse bright channel, the difference between secondary sparse dark channel image and secondary sparse bright channel image can be calculated. Thus, an image edge selection method can be obtained [27].

$$I(x) = sB(I)(x) - sD(I)(x). \tag{27}$$

Figure 3 shows the image edges extracted by five different methods in an ultrasonic blurred image.

It can be seen from Fig. 3, the image edge extracted from horizontal gradient and Laplace gradient operator is not complete while the image edge extracted from Canny operator and Sobel operator also extracts other regions outside the edge as edges. However, the method in this paper can better extract the edge of fuzzy image without mistakenly extracting other regions outside the edge [28].

4. ULTRASONIC IMAGE DEBLURRING MODEL WITH DOUBLE CONSTRAINTS

Obtain the gradient of ultrasonic image in RGB orthogonal color space with color constancy. Then, the edge is extracted by using the local information of quadratic sparse dark channel and quadratic sparse bright channel images. Finally, a new double regularization constraint is proposed by combining L1 norm with L2 norm. And the extracted edge and the new double regularization constraint are added to the ultrasonic image degradation model [29].

4.1 *Model Proposed*

The image deblurring model proposed in this paper is as follows:

$$(I', K') = \arg\min_{I,K} \left| \sum_{\partial \in \lambda} \partial I \otimes k - \sum_{\partial \in \lambda} \partial I \otimes k - \sum_{\partial \in \lambda} \partial I \beta \right|. \tag{28}$$

$\lambda = (\partial^0, \partial^c)$ refers to the image itself; ∂^0 refers to the image itself; ∂^c is the gradient extracted from RGB orthogonal ultrasonic space. I' and β' represent the edges of a clear image and a blurred image respectively. λ represents the weight parameter, and $0 \leq \lambda \leq 1$.

4.2 *Semi Quadratic Splitting Solution of Model*

Because there are two unknowns: clear image I and fuzzy kernel K in the model (4.14), it is difficult to directly find its solution. Therefore, this paper adopts semi quadratic splitting method and alternating minimization method to turn the optimization problem of model (28) into the following two subproblems.

$$k' = \arg\min_{k} \left| \sum_{\partial \in \lambda} \partial I \otimes k - \sum_{\partial \in \lambda} \partial \beta \right| + \gamma \|k\|^2 \tag{29}$$

$$I' = \min_{I} \left| \sum_{\partial' \in \lambda} \partial' I' \otimes k - \sum_{\partial' \in \lambda} \partial' \beta \right| + \lambda \|k\|^2. \tag{30}$$

Introduce the proposed quadratic sparse extreme channel prior term (30) into the image deblurring framework. The proposed image deblurring objective function becomes:

$$\{I', k'\} = \arg\min_{I,K} \|I \otimes k - B\|_2^2 + \gamma p(k) + \theta p(I). \tag{31}$$

Where $p(k)$ and $p(I)$ are the blur kernel prior and the quadratic sparse extreme channel prior of the image respectively. γ, θ is the weight parameter.

4.3 *Estimation of Fuzzy Kernel K*

In fact, IRLS approximately replaces p norm with 2 norms and transforms it into a weighted linear least squares problem. Therefore, in order to solve the problem that it is difficult to calculate the regular term L_P in the kernel estimation problem, the estimation model of using IRLS method to solve the fuzzy kernel K can be written as follows:

$$I' = \min_I \left| \sum_{\partial' \in \lambda} \partial' I' \otimes k - \sum_{\partial' \in \lambda} \partial' \beta \right| + \lambda \|k\|^t. \tag{32}$$

∂', β is the parameter and $\lambda\|k\|^t$ is the weight of the tth iteration of the fuzzy kernel. Its weight is defined as follows:

$$\begin{cases} w_k^{(0)} = 1 \\ w_k^{(t)} = \dfrac{1}{\max(|\nabla I|, 0.01)}. \end{cases} \tag{33}$$

4.4 *Solution of Clear Image I*

Because the algorithm in this paper is based on RGB orthogonal color space, the intermediate image estimation is also an ultrasonic image, which is different from the traditional calculation. In this paper, when estimating the intermediate image, each color channel of ultrasonic image must be solved, and the K in the formula is the same [30]. IRLS can transform the norm into a weighted linear least squares problem. Therefore, IRLS method is used to solve the intermediate image I. And its estimation model is as follows:

$$i^{(t+1)} = \min \left\| \sum_{\partial \in 0} \partial I \otimes k - \sum_{\partial \in 0} \partial B \right\|^2 + \mu \|\nabla I\|^2 + \lambda w_i^{(t)} \|\nabla I\|^2. \tag{34}$$

μ, λ is the parameter and $w_t^{(t)}$ is the weight of the tth iteration of the intermediate image.

$$\begin{cases} w_k^{(0)} = 1 \\ w_k^{(t)} = \dfrac{1}{\max(\Delta I \mid 0.001)}. \end{cases} \tag{35}$$

The model (34) may cause gradient effects and destroy textures. In order to preserve the sharp edges in the restored ultrasound image, this paper combines the adaptive weighting space, and the final deblurring ultrasound image estimation model is:

$$I = \min_i \|B - k \otimes I\| + w_x^{(t)} \|\partial_x I\| + w_y^{(t)} \|\partial_y I\|. \tag{36}$$

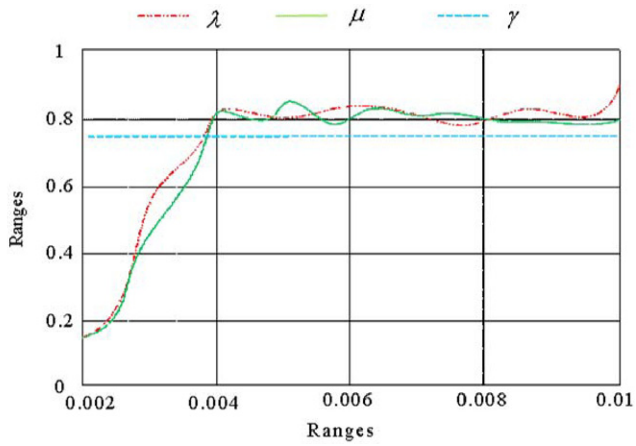

Figure 4. Sensitivity analysis of parameters λ, μ, γ in algorithm.

IRLS is used to transform 1 norm into a weighted linear least squares problem, so the final deblurring ultrasonic image estimation model can be written as:

$$I^{(t+1)} = \min_t \|B - k \otimes I\|_2^2 + w_x^{(t)} \|\partial_x I\|^2 + w_y^{(t)} \|\partial_y I\|^2. \tag{37}$$

The weight of $\partial_x I$ and $\partial_y I$ is defined as:

$$\begin{cases} w_0^{(0)} = 1 \\ w_y^{(0)} = 1. \end{cases} \tag{38}$$

5. EXPERIMENTAL ANALYSIS

The experimental data set uses the fuzzy ultrasonic image data set to test the algorithm. The fuzzy ultrasound image data set contained common carotid artery (CCA) images of 10 volunteers with different body weights (mean weight 76.5 ± 9.7 kg) and ages (mean age 27.5 ± 3.5 years). The fuzzy ultrasound image data set contains 84 CCA longitudinal B-ultrasound images.

5.1 *Parameter Setting*

In this paper, the blind deblurring model mainly has three parameters: λ, μ, γ. In order to analyze the effect of these parameters, 20 fuzzy images are used as the test, and the similarity of fuzzy kernel is used as the measurement standard. Figure 4 shows the influence of parameters λ, μ, γ on the deblurring algorithm in this paper.

For each parameter, its function is verified by fixing other parameters. For the parameter λ, its value is limited between 0 and 0.01, in which the sampling step is 0.0005. Fig. 4 shows the impact on the deblurring algorithm of λ. When the value range is $[0.001, 0.01]$, the deblurring algorithm in this paper has certain robustness. Similarly, set the value of μ is between 0 and 0.01, in which the sampling step is 0.0005; When the value range of μ is $[0.002, 0.01]$, the defuzzification algorithm in this paper has certain robustness. Set the value of γ is 0 to 1, in which the sampling step is 0.01; when the value range of γ is $[0.01, 1]$, the deblurring algorithm in this paper has certain robustness.

Algorithm description

Algorithm 1: steps of ultrasonic image deblurring algorithm with double constraints

Input:

Blur image β and kernel size

Step 1: Estimate the fuzzy kernel

The number of image pyramids n is determined according to the size of the kernel;

$for\ i = 1 : n$

Downward sampling β according to the current image pyramid and obtain β_i;

$for\ innerItr = 1 : m$

Solve the ultrasonic image gradient according to formula (26);

Solve the image edge according to formula (27);

$for\ i = 1 : Itr$

Solve k' **with** model (32);

$k \leftarrow k'$;

End

Solve the intermediate image I_i according to formula (34);

$t \leftarrow t/1.1, \quad \theta \leftarrow \theta/1.1$;

End

Upward sampling image iI and set $I_{i+1} \leftarrow I_i$;

End

Output: intermediate image I_i and blur kernel k;

Step 2: estimate the final deblurring image I according to formula (35);

Output: deblurring image I and blur kernel k;

For the parameters $\gamma = 0.01$ in model (33) and $\lambda = 0.004$, $\mu = 0.004$ in model (35), the number of iterations in IRLS iteration space is $t = 3$. A negative value will be generated when solving the model (33). Therefore, for the estimated fuzzy kernel, the negative element is set to 0 and renormalized. In the final clear image restoration process, each color channel is processed separately and its blur kernel k is the same.

5.2 *Analysis of Experimental Results*

In order to illustrate the feasibility and advantages of the algorithm proposed in this paper, this section will use the edge selection method proposed in this paper to deblur the image with several other edge extraction methods (horizontal step, Canny operator, Sobel operator and Laplace gradient operator), and compare the results. The experimental results are shown in Figure 5.

It can be seen from Fig. 5: the edge of the image deblurring based on Canny operator rings, and the image deblurring based on Sobel operator has a blocking effect. It can be seen visually that the image information deblurring based on the image selected in this study is clearer. Therefore, the edge selection method proposed in this paper is feasible.

In order to further illustrate the excellence of the proposed algorithm in deblurring blurred ultrasonic images, the image deblurring algorithms of five different edge extraction methods are deblurred. Then the deblurring results are evaluated by six evaluation indexes. The evaluation results are shown in Table I.

Table I. Comparison of deblurring performance of several edge extraction algorithms.

	PSNR	SSIM	VIF	FSIM	RG	BIQI
Horizontal first-order gradient	32.5	0.82	0.57	0.63	0.88	34.6
Canny operator	34.2	0.78	0.62	0.67	0.93	35.6
Sobel operator	38.1	0.83	0.58	0.68	0.92	38.5
Laplas gradient operator	37.2	0.87	0.59	0.59	0.94	37.6
At the edge of this article	39.9	0.98	0.89	0.88	0.98	38.9

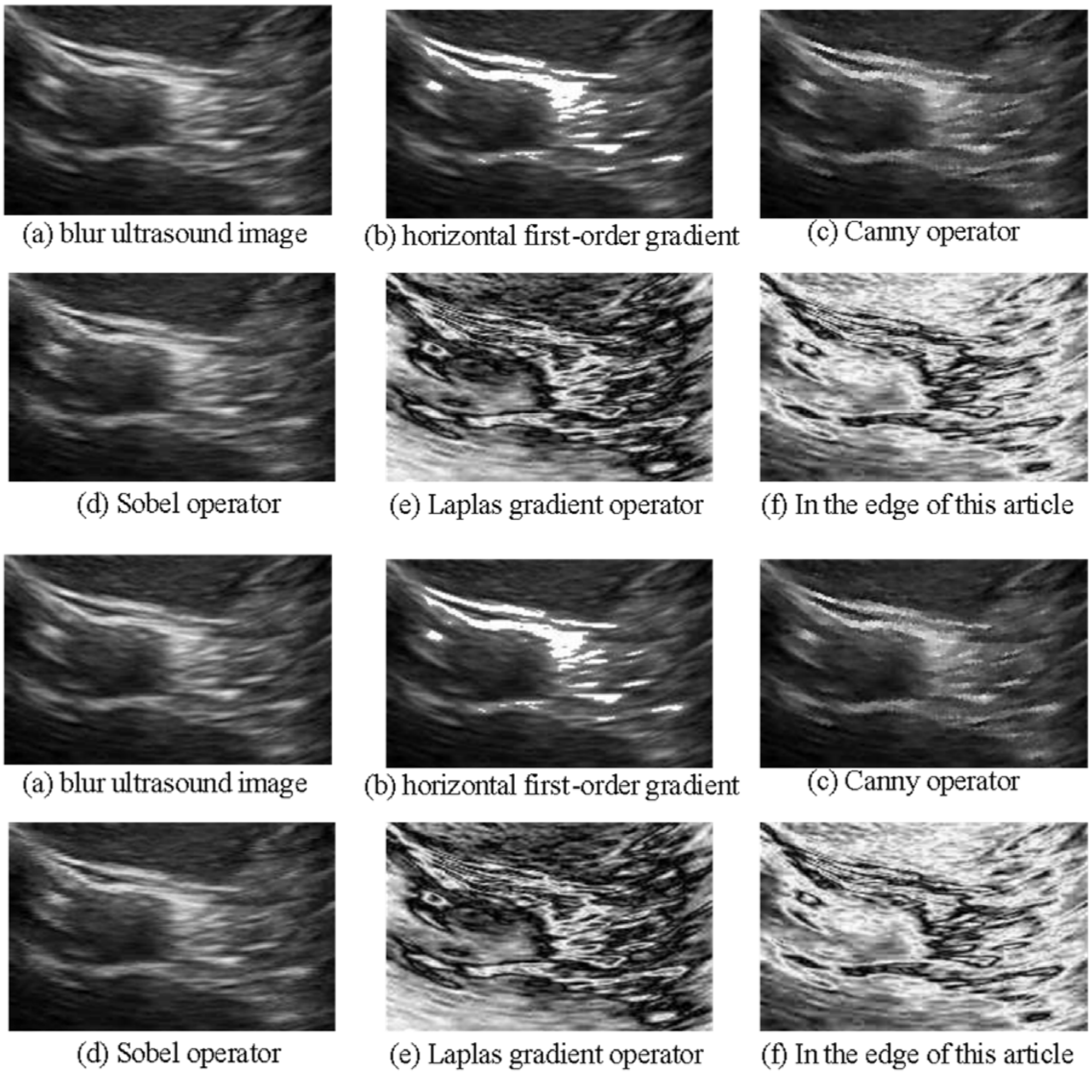

Figure 5. Comparison of deblurring results of blurred ultrasonic images with different edge selection.

The results show that the image deblurring algorithm based on edge selection in this paper is the highest in the six evaluation indexes. Therefore, it shows that the edge extraction method is effective.

The proposed algorithm is tested on CCA fuzzy ultrasonic image data set. It is compared with six other fuzzy image deblurring algorithms (Krishnan algorithm, Yan algorithm, Pan algorithm, Hu algorithm, Bai algorithm and Wen algorithm). Figure 6 shows the experimental results of seven algorithms for deblurring CCA blurred ultrasonic images.

The upper right corner of the deblurring experimental results is the fuzzy kernel (size is 5×5) estimated by the corresponding algorithm. The experimental results shown in Fig. 6 show that Yan algorithm has obvious noise points, pan algorithm has obvious ringing phenomenon and Bai algorithm has obvious artifact phenomenon. The algorithm proposed in this paper has a good effect on deblurring blurred ultrasonic images.

In order to further illustrate the excellence of the algorithm proposed in this paper in deblurring fuzzy ultrasonic images, seven kinds of fuzzy image deblurring algorithms are used to deblurring fuzzy ultrasonic images on CCA data set. And then six evaluation indexes are used to evaluate the quality of deblurring results. The evaluation results are shown in Table II.

The first four evaluation indexes (PSNR, SSIM, VIF, FSIM) are commonly used full reference evaluation indexes, and the last two evaluation indexes (RG, BIqI) are new non-reference evaluation indexes. From the evaluation results in Table II, it can be seen that compared with the latest algorithm (Wen algorithm), the method in this paper has the following advantages: the peak signal-to-noise ratio is increased by 7%; the structural similarity value is increased by 6%; the visual information fidelity is increased by 14%; the feature similarity value is increased by 4%; the resolution gain is increased by 4% and the new blind image quality evaluation value is increased by 22%. Therefore, the six evaluation index

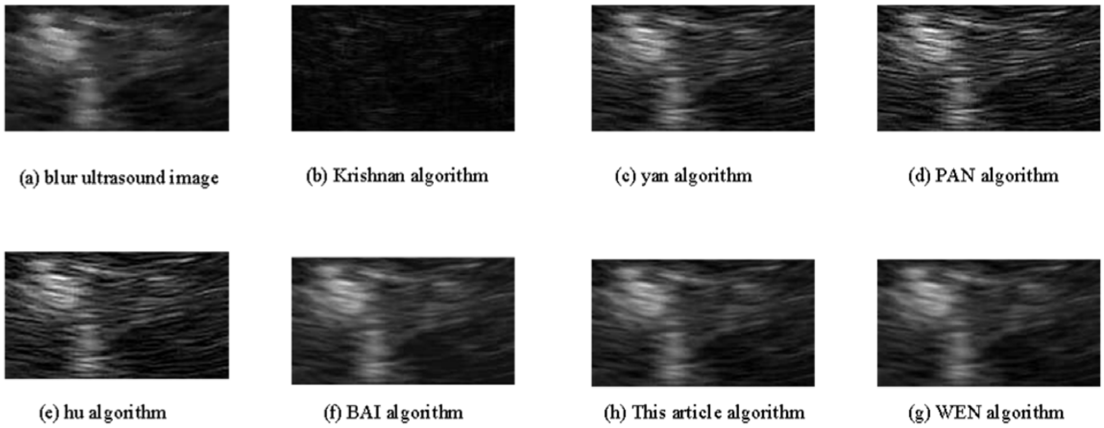

Figure 6. Comparison of deblurring results of blurred ultrasound images on CCA dataset.

Table II. Comparison of defuzzification performance of seven algorithms.

	PSNR	SSIM	VIF	FSIM	RG	BIQI
Krishnan algorithm	37.2	0.78	0.65	0.82	0.82	34.5
Yan algorithm	34.8	0.74	0.71	0.81	0.83	35.2
PAN algorithm	35.6	0.69	0.69	0.79	0.87	34.8
HU algorithm	38.2	0.71	0.77	0.77	0.79	34.6
BAI algorithm	35.6	0.75	0.78	0.76	0.82	35.1
Wen algorithm	36.7	0.77	0.68	0.81	0.81	36.5
Algorithm	41.2	0.99	0.97	0.97	0.96	39.9

values of the proposed algorithm are basically better than the other six algorithms. It shows that compared with the other six algorithms the proposed algorithm is effective for distorted fuzzy ultrasonic images, which can obtain better deblurring images.

6. CONCLUSION

In this paper, a double constrained ultrasonic image deblurring method is proposed. Firstly, RGB ultrasonic space is transformed into RGB orthogonal ultrasonic space with better color constancy; secondly, based on quadratic sparse dark channel and quadratic sparse bright channel, a more effective edge extraction method is used; then, a double constrained ultrasonic image deblurring algorithm is proposed, which has better constraints on the sparsity and continuity of image deblurring; finally, an image smoothing model based on image spatial information is established.

Due to the increase of quadratic sparsity operation of the bright channel and dark channel, the running time of the proposed algorithm increases. At the same time, because the fuzzy ultrasound image in this paper only selects the carotid ultrasound image, a large number of experiments need to be carried out on different types of ultrasound images in order to make the algorithm proposed in this paper more universal.

REFERENCES

[1] Y. Liao, W. Li, J. Cui, and W. Gong, "Blur kernel estimation model with combined constraints for blind image deblurring," *Proc. 2018 Digital Image Computing: Techniques and Applications (DICTA)* (IEEE, Piscataway, NJ, 2018), pp. 1–8.

[2] L. Chen, F. Fang, T. Wang, and G. Zhang, "Blind image deblurring with local maximum gradient prior," *Proc. IEEE/CVF Conf. on Computer Vision and Pattern Recognition* (IEEE, Piscataway, NJ, 2019), pp. 1742–1750.

[3] K. Zhou, P. Zhuang, J. Xiong, J. Zhao, and M. Du, "Blind image deblurring with joint extreme channels and L0-Regularized Intensity And Gradient Priors," *Proc. 2020 IEEE Int'l. Conf. on Image Processing (ICIP)* (IEEE, Piscataway, NJ, 2020), pp. 873–1177.

[4] D. Yang, X. J. Wu, and H. Yin, "Blind image deblurring via enhanced sparse prior," J. Electron. Imaging **30**, 023031 (2021).

[5] H. Zhang, B. Yuan, B. Dong, and Z. Jiang, "No-reference blurry image quality assessment by structural similarity index," Appl. Sci. **8**, 2003 (2018).

[6] W. Wu, C. Hong, Y. Xie, and L. Chen, "Image quality assessment based on BIQI with gray beep," *Proc. 2018 IEEE Int'l. Conf. on BigData (Big Data)* (IEEE, Piscataway, NJ, 2018), pp. 4632–4639.

[7] F. Z. Ou, Y. G. Wang, and G. Zhu, "A novel blind image quality assessment method based on refined natural scene statistics," *Proc. 2019 IEEE Int'l. Conf. on Image Processing (ICIP)* (IEEE, Piscataway, NJ, 2019), pp. 1004–1008.

[8] X. Y. Yu and W. Xie, "Single image blind deblurring based on salient edge-structures and elastic-net regularization," J. Math. Imaging Vis. **62**, 1049–1061 (2020).

[9] X. Chen and Q. Zhu, "A fast FFT-based iterative algorithm for image deblurring with anti-reflective boundary conditions," *Proc. 2018 Int'l. Conf. on Network, Communication, Computer Engineering (NCCE 2018)* (Atlantis Press, Dordrecht, 2018), pp. 446–456.

[10] L. Hehn, S. Tilley, F. Pfeiffer, and J. W. Stayman, "Blind deconvolution in model-based iterative reconstruction for CT using a normalized sparsity measure," Phys. Med. Biol. **64**, 215010 (2019).

[11] Z. Hu, S. Cho, J. Wang, and M. H. Yang, "Deblurring low-bright images with light streaks," *Proc. IEEE Conf. on Computer Vision and Pattern Recognition* (IEEE, Piscataway, NJ, 2014), pp. 3382–3389.

[12] Q. Shu, C. Wu, Q. Zhong, and R. W. Liu, "Alternating minimization algorithm for hybrid regularized variational image dehazing," Opt. – Int'l. J. Bright Electron Opt. **185**, 943–956 (2019).

[13] K. Cheng, J. Du, H. Zhou, D. Zhao, and H. Qin, "Image super-resolution based on half quadratic splitting," Infrared Phys. Technol. **105**, 103193 (2020).

[14] Y. Han and J. Kan, "Blind color-image deblurring based on color image gradients," Signal Process. **155**, 14–34 (2019).

[15] Y. Han and J. Kan, "Blind image deblurring based on local edges selection," Appl. Sci. **9**, 3274 (2019).

[16] Y. Bai, G. Cheung, X. Liu, and W. Gao, "Graph-based blind image deblurring from a single photograph," IEEE Trans. Image Process. **28**, 1404–1418 (2018).

[17] H. Queen, L. Y. Yan, and N. Yunjun, "Based on fuzzy nuclear surprise precederation treatment," J. Anhui Univ. (Natural Science Edition) **43**, 43–77 (2019).

[18] F. Wen, R. Ying, Y. Liu, P. Liu, and T. K. Truong, "A simple local minimal intensity prior and an improved algorithm for blind image deblurring," *IEEE Transactions on Circuits and Systems for Video Technology* (IEEE, Piscataway, NJ, 2020), pp. 1–1.

[19] T. Guo, H. S. Mousavi, T. H. Vu, and V. Monga, "Deep wavelet prediction for image super-resolution," *2017 IEEE Conf. on Computer Vision and Pattern Recognition Workshops (CVPRW)* (IEEE, Piscataway, NJ, 2017), pp. 1100–1109.

[20] B. Lim, S. Son, H. Kim, S. Nah, and K. Mu Lee, "Enhanced deep residual networks for single image super-resolution," *2017 IEEE Conf. on Computer Vision and Pattern Recognition Workshops (CVPRW)* (IEEE, Piscataway, NJ, 2017), pp. 1132–1140.

[21] Y. Zhang, K. Li, K. Li, L. Wang, B. Zhong, and Y. Fu, "Image super-resolution using very deep residual channel attention networks," in *Computer Vision – ECCV 2018. ECCV 2018*, edited by V. Ferrari, M. Hebert, C. Sminchisescu, and Y. Weiss, Lecture Notes in Computer Science (Springer, Cham, 2018), Vol. 11211, pp. 294–310.

[22] Z. Li, J. Yang, Z. Liu, X. Yang, G. Jeon, and W. Wu, "Feedback network for image super-resolution," *2019 IEEE/CVF Conf. on Computer Vision and Pattern Recognition (CVPR)* (IEEE, Piscataway, NJ, 2019), pp. 3862–3871.

[23] Y. Zhang, Y. Tian, Y. Kong, B. Zhong, and Y. Fu, "Residual dense network for image super-resolution," *2018 IEEE/CVF Conf. on Computer Vision and Pattern Recognition* (IEEE, Piscataway, NJ, 2018), pp. 2472–2481.

[24] Y. Yan, W. Ren, Y. Guo, R. Wang, and X. Cao, "Image deblurring via extreme channels prior," *Proc. IEEE Conf. on Computer Vision and Pattern Recognition* (IEEE, Piscataway, NJ, 2017), pp. 4003–4011.

[25] D. Gong, M. Tan, Y. Zhang, A. Van Den Hengel, and Q. Shi, "Self-paced kernel estimation for robust blind image deblurring," *Proc. IEEE Int'l. Conf. on Computer Vision* (IEEE, Piscataway, NJ, 2017), pp. 1661–1670.

[26] S. Chengyang, M. Hai, H. Yahong, and S. Weiguo, "Study on the defunction of vina filter image based on adaptive of RGB channel," Comput. Meas. Control **27**, 215–219 + 238 (2019).

[27] C. Mei, C. Guobin, and L. Chao, "Blurred image blind reset method of dark pixel prior art," Comput. Eng. Appl. **56**, 213–519 (2020).

[28] N. N. Zhao, Q. Wei, A. Basarab, D. Kouamé, and J. Y. Tourneret, "Single image super-resolution of medical ultrasound images using a fast algorithm," *Proc. 2016 IEEE 13th Int'l. Symposium on Biomedical Imaging (ISBI)* (IEEE, Piscataway, NJ, 2016), pp. 473–476.

[29] J. S. Pan, D. Q. Sun, H. Pfister, and M. H. Yang, "Blind image deblurring using dark channel prior," *Proc. IEEE Conf. on Computer Vision and Pattern Recognition* (IEEE, Piscataway, NJ, 2016), pp. 1628–1636.

[30] K. Ohashi and T. Ishida, "Deblurring algorithm for blurred images caused by patient motion in radiography," Nihon Hoshasen Gijutsu Gakkai Zasshi **72**, 961–969 (2016).